

## Tip-Sample Forces in Atomic Force Microscopy: Interplay between Theory and Experiment

Sergey Belikov, John Alexander, Craig Wall, and Sergei Magonov

NT-MDT Development Inc., 430 W. Warner Road, Tempe, AZ 85284, U.S.A.

### ABSTRACT

Several examples of Atomic Force Microscopy imaging in the oscillatory resonant and non-resonant modes are analyzed with a theoretical description of tip-sample force interactions. The problems of high-resolution imaging and compositional mapping of heterogeneous polymers are considered. The interplay with theory helps the experiment optimization and rational understanding of the image contrast.

### INTRODUCTION

Over the past 20 years Atomic Force Microscopy (AFM) has evolved from a high-resolution and low-force imaging tool to a family of comprehensive techniques also covering local measurements of different sample properties. The theoretical understanding of tip-sample interactions, however, lags far behind practical experience and instrumental developments in AFM. This situation needs to be changed and several aspects of interplay between the theory and experiment are outlined below. There are several DC and AC AFM modes, in which the probe deflection or changes of its oscillation parameters are utilized for instrument control and data harvesting. A rational understanding of tip-sample forces in these modes can be elucidated by solving the Euler-Bernoulli equations that describe the oscillating probe interacting with a sample. The Krylov-Bogoliubov-Mitropolsky asymptotic approach based on separation of the fast and slow changing variables led to the solution expressed by two equations containing four unknowns (central probe position -  $Z_c$ , imaging amplitude, frequency, phase -  $\theta$ ). By fixing two of the unknowns, one can realize the amplitude modulation (AM), frequency modulation (FM) and other modes [1]. In AM these equations are as follows:

$$\sin \theta = \frac{1}{N} \int_0^{\pi} [F_a - F_r] (Z_c + A_{sp} \cos y) \sin y dy + \frac{A_{sp}}{A_0} \quad (1)$$

$$\cos \theta = -\frac{1}{N} \int_0^{\pi} [F_a + F_r] (Z_c + A_{sp} \cos y) \cos y dy \quad (2)$$

Where  $A_0$  – the free probe amplitude,  $A_{sp}$  – the set-point amplitude;  $Z_c$  – a central position of the cantilever over a surface during oscillations, and  $N = \pi A_0 k / Q$  ( $k$  and  $Q$  – spring constant and quality factor of the probe at 1<sup>st</sup> flexural resonance),  $F_a$  and  $F_r$  – the tip-sample forces experienced by a probe in the approach and retract to the surface parts of the oscillatory cycles.

The integrals in (1) -  $I_{\sin}$  and in (2) -  $I_{\cos}$  can be connoted as the dissipative and conservation integrals, respectively. In the case of conservative forces the dissipative integral is nullified and the first equation is simplified. Knowledge of a relationship between the force and specific surface properties, is essential for their quantitative extraction from AFM data.

Besides the classification of the AFM oscillatory modes, this theoretical method was also

implemented in an AFM simulator, which has been beneficial in generating atomic-scale images with single defects, for tips of different sizes, and various force levels [2]. The general nature of the above equations allow their use not only for analysis of mechanical tip-sample forces but also for evaluation of conservative electrostatic interactions and retrieval of quantitative dielectric permittivity from  $dC/dZ$  measurements of thin polymer films [3]. Here we extend the theoretical analysis of AFM studies by considering the high-resolution imaging of calcite crystals in water and compositional mapping of heterogeneous polymers with resonant and non-resonant oscillatory modes, by recording probe-sample dissipation maps and by using bimodal excitation.

## **EXPERIMENTAL DETAILS**

The AFM images discussed below we obtained with the NEXT scanning probe microscope developed by NT-MDT (Zelenograd, Russia), which differs from its predecessors by a low noise of optical detection (25 fm/ $\sqrt{\text{Hz}}$  for 100 micron long probes), low noise high-voltage amplifier and by the integration of 5 lock-in amplifiers enabling multi-frequency mechanical and electric modes. An additional fast data acquisition and control module was applied for enabling the non-resonant oscillatory mode. The materials used in the experiments were purchased from different sources [calcite crystals - from Ward Scientific Inc., polystyrene (PS), polybutadiene (PB) and triblock copolymer polystyrene-*b*-polybutadiene - *b* – polystyrene (SBS) - from Polymer Source Inc.]. The samples for AFM studies were prepared by cleavage of calcite crystals and spin cast of SBS, PS+PB solutions in toluene on flat Si substrates. A sample of polydiethylsiloxane was prepared by rubbing this polymer on Si substrate. A sample with polymer brush macromolecules on Si substrate is courtesy of Prof. S. Sheiko (UNC). Commercial Si probes with spring constants in the 4 - 40 N/m range (NSG30, NSC14) were used in the studies. The thermal resonance procedure was used for finding the probe resonance in water prior to imaging of calcite crystals. The crystals were immersed for 1.5 hour prior to imaging. Modeling of the tip-sample force interactions was performed with LabVIEW software.

## **RESULTS AND DISCUSSION**

### **High-resolution imaging**

Atomic-scale imaging with scanning probe methods was first realized with scanning tunneling microscopy and later was expanded to studies of non-conducting surfaces with AFM initially in the contact mode and recently in the oscillatory FM and AM modes. Our previous experience in atomic-scale studies with STM and contact mode AFM has shown that the visualization of sub-nm lattices and sometimes even single defects is best achieved on clean crystallographic surfaces of layered materials. One overlooked specific of SPM studies is that zooming from large to atomic-scale areas is accompanied by an effective increase of the local dwell time of the probe and thus enhanced force interactions. Therefore a reduction of scanning area, which leads to an increase in the tip-sample force, might lead to the creation and evolution of top layer defects resulting in layer-by-layer material removal, temporarily revealing a new and less defective surface, until the process is repeated. The same picture is common for AM imaging as demonstrated by the results obtained on a calcite surface under water, figure 1. In the large scans, an area of the bottom layer has increased due to continuous destruction of the top

layer. The loose material present on the surface is invisible, being pushed by the probe. Imaging of a calcite crystal under water was performed with a relatively small amplitude ( $A_0 = 1$  nm,  $A_{sp} = 0.8$  nm) and in some instances it was possible to collect an atomic-scale lattice image on the top surface without its damage. In most cases, however, scanning was accompanied by layer-by-layer damage that is manifested by multiple steps created during the scan. One of the steps with an identical lattice pattern on the terraces is seen in the height image. The phase image, which is less sensitive to the topographic step, clearly reveals the crystallographic order of the calcite.

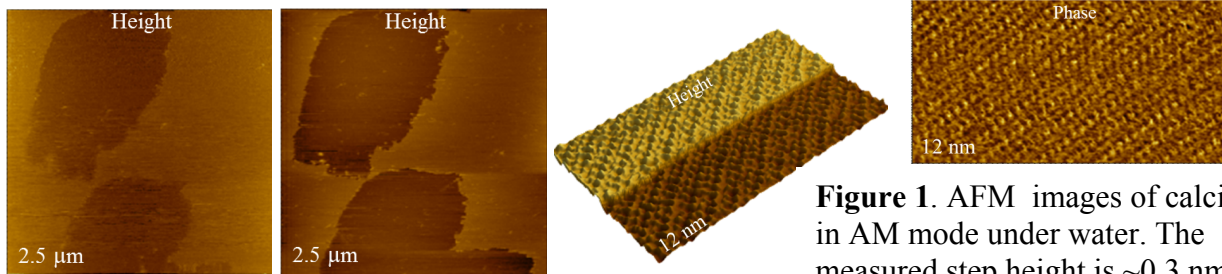


**Figure 1.** AFM images of calcite in AM mode under water. The measured step height is  $\sim 0.3$  nm

These results underline the importance of quantitative estimates of the maximal tip force and its optimization to make the atomic-scale imaging and detection of single defects a routine procedure. We have performed such estimates for imaging in air using the above theoretical approach. The tip-force at the lowest oscillation point was estimated by finding the related Z-coordinate and applying the Hertz model. The plot in figure 2 (left) describes how the maximum tip-force changes with  $A_{sp}$  for samples with different elastic modulus. The tip-force reaches its maximum at  $A_{sp} \sim 0.5 \times A_0$  and drops at lower  $A_{sp}$  due to a gradual shift of the effective probe resonance. Our estimate of the tip-force during imaging of calcite (elastic modulus  $\sim 72$  GPa) under water gives the maximal force value around 27 nN and the deformation of 0.2 nm. As we learned, imaging at this force is destructive and further reduction of amplitude to 0.1 nm that brings the maximal force to 2 nN and the deformation to 0.04 nm might be needed.

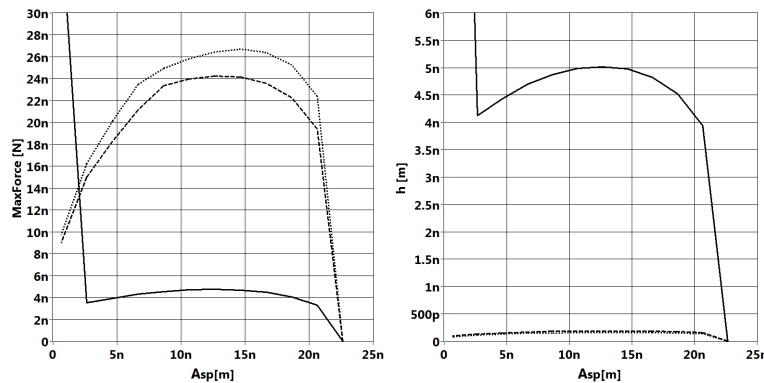


**Figure 2.** The plots of maximal tip-force (left) and sample depression (right) calculated with the Hertz model at different  $A_{sp}$  and for the samples with 100 MPa elastic modulus (solid line), with 2 GPa elastic modulus (dashed line) and with 70 GPa elastic modulus (dotted line).

### Comparing imaging with resonant and non-resonant oscillatory modes

In the development of AFM modes, researchers have renewed their attention to non-resonant imaging modes using the probe deflection for topography control [4]. The images of the same locations of polymer brushes and SBS film were obtained in AM mode at the probe resonance (50 – 400 kHz) and in the non-resonant mode at low frequency (1-3 kHz). The images of polymer brushes are quite different. In the AM height image, these macromolecules with

numerous side chains are seen as bulky structures with the elevations  $\sim 10$  nm, figure 3. The force increase did not show much height depression when  $A_{sp}$  was lowered. The macromolecules are much thinner in the image obtained in the non-resonant mode. They are macromolecules only 3 nm tall, and this indicates that the tip force depresses the objects. The high-force level imaging in the non-resonant mode is also confirmed by study of SBS film. It has been established that the SBS surface is enriched by PB blocks, which have lower surface energy. Therefore, the micro-phase separation becomes evident in AFM height and phase images only when at elevated force operation the probe depresses the top layer [5]. This is demonstrated in the height images in figure 4 (left, center). The height image of the same location (figure 4, right), which was obtained in the non-resonant mode, also reveals the micro-phase separation. The theoretical estimates showed that for the same probe ( $\sim 4$  N/m) the maximal force in AM imaging of SBS is close to the lowest force in the non-resonant mode.

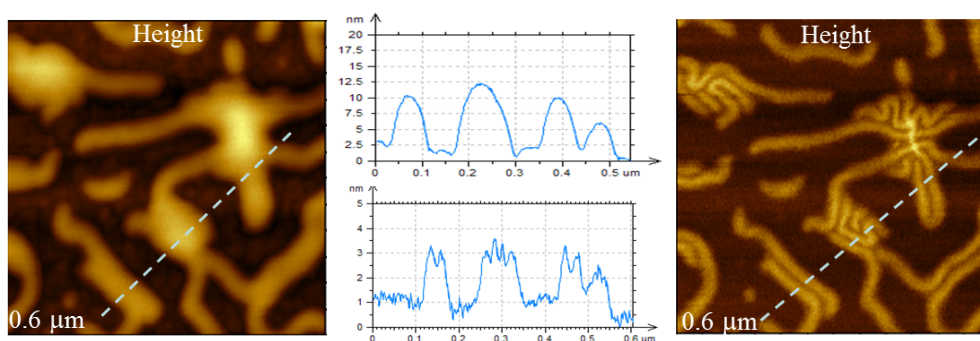


**Figure 3.** Height images and cross-sections of polymer brush macromolecules obtained in AC (left) and the non-resonant mode (right).

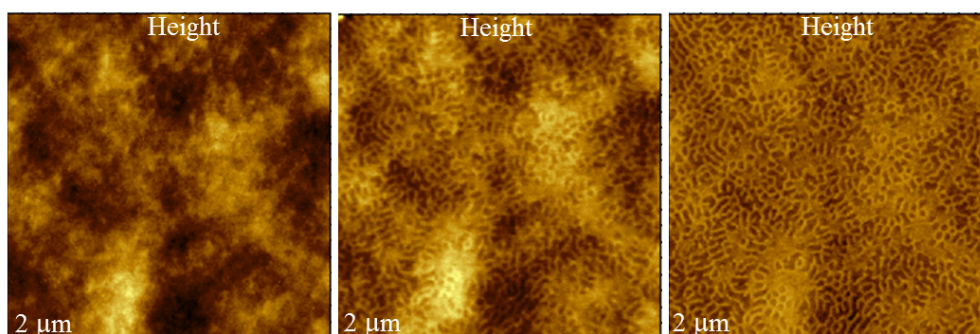


**Figure 4.** Height images of SBS triblock copolymer film obtained in AC (left, center) and the non-resonant mode (right).

The presented results show that imaging in non-resonant mode is characterized by a higher tip force level yet in practical AFM studies these methods can complement each other.

### Conservative and dissipative interactions in AFM

The use of a rational model describing the depression or penetration of the AFM probe in to soft samples such as polymers or biological specimens is essential for the extraction of quantitative mechanical properties at small scales. Unfortunately, the solid-state deformation models (Hertz, Sneddon, JKR, DMT), which are used in AFM nanomechanical studies, describe the conservative force interactions with or without adhesion. This is unfortunate because most of the polymer materials exhibit dissipative mechanical behavior and their viscoelasticity is routinely characterized at the macroscopic scale. Another complication in AFM of heterogeneous systems is that the phase images, in which the individual constituents are best resolved, are

difficult to interpret in terms of mechanical and adhesive properties. Some semi-empirical phase/elastic modulus relations have been used in practical work. In AM mode, the probe dissipation expressed by  $\tan\delta$  was suggested to describe the local viscoelasticity of polymer samples [6]. From equations (1) - (2) we define the probe-sample dissipation as the  $I_{\sin}$  integral and  $\tan\delta$  as the ratio of the  $I_{\sin}$  and  $I_{\cos}$  integrals. The dissipation and  $\tan\delta$  maps of a PS/PB blend are presented together with the height and phase images in figure 5. The images show that the dissipation and  $\tan\delta$  contrast is similar to the phase contrast. Therefore, the value of the probe dissipation and  $\tan\delta$  measurements relies on finding their relation to sample viscoelasticity. We should not exclude that other AFM experiments (an indent recovery [7], or frequency-dependent local dielectric response) more directly correlate with polymer dissipative properties.

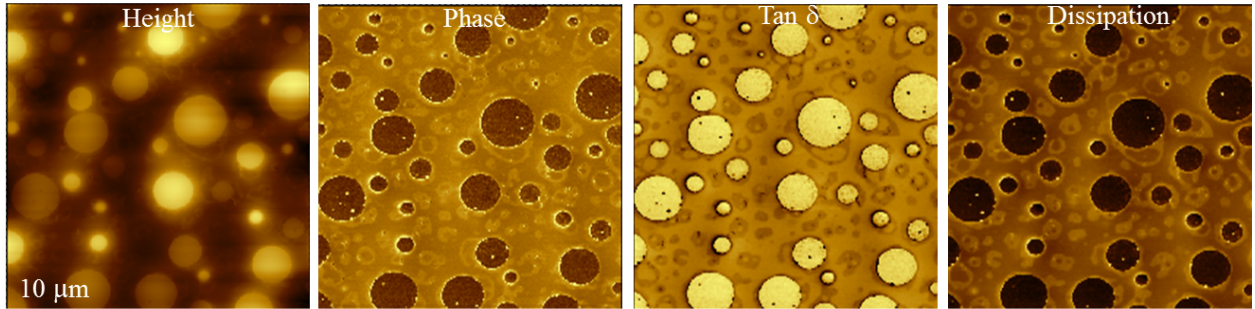


**Figure 5.** Images of PS/PB blend with the components' separation in contrast of various origin.

### **Bimodal excitation**

The expansion of AFM instrumental capabilities is being stimulated by the development of multi-frequency techniques. The techniques advance local electric studies by enabling single-pass measurements. Several attempts were made to enhance nanomechanical experiments, and here we consider the effect of bimodal excitation, in which the probe interactions with a sample are generated and measured at two resonant frequencies [8]. The tip-sample interactions when the probe is simultaneously driven at the 1<sup>st</sup> and 2<sup>nd</sup> flexural modes were recorded in amplitude-versus-distance curves and images of a sample of PDES, whose structural organization has been explored earlier with AFM [9]. The cross-effects between the amplitude responses at both flexural modes were observed, and complete damping of the 1<sup>st</sup> softer mode was noticed even at high  $A_{sp}$  when the 2<sup>nd</sup> mode was employed for surface tracking, because the 2<sup>nd</sup> mode is much stiffer. Therefore, we have performed imaging at the 1<sup>st</sup> mode and recorded the responses of phase signals of both modes, figure 6. The related phase images of the PDES patches on Si reveal lamellar aggregates embedded into an amorphous material and the contrast of these components is different from the contrast of the substrate. The phase contrast of the 2<sup>nd</sup> mode shows more composition details. The equations (1) and (2) of the probe response to the single excitation (conservative case) can be expressed as:

$$1 - \left( \frac{A_1}{A_{10}} \right)^2 - \left( \frac{2}{N} \int_0^\pi F(\mathbf{Z}_c + A_1 \cos \gamma_1) \cos \gamma_1 d\gamma_1 \right)^2 = 0 \quad (3)$$

where  $A_1 = A_{sp}$  and  $A_{10} = A_0$  for 1<sup>st</sup> mode. Similar equations for the excitation of the 1<sup>st</sup> and 2<sup>nd</sup>

modes are as follows:

$$\left\{ 1 - \left( \frac{A_1}{A_{10}} \right)^2 - \left( \frac{1}{2\pi} \int_0^{2\pi} \left[ \frac{2}{N_1} \int_0^\pi F(\mathbf{Z}_c + \mathbf{A}_2 \cos \gamma_2 + A_1 \cos \gamma_1) \cos \gamma_1 d\gamma_1 \right] d\gamma_2 \right)^2 = 0 \right. \quad (4)$$

$$\left. 1 - \left( \frac{A_2}{A_{20}} \right)^2 - \left( \frac{1}{2\pi} \int_0^{2\pi} \left[ \frac{2}{N_2} \int_0^\pi F(\mathbf{Z}_c + A_1 \cos \gamma_1 + \mathbf{A}_2 \cos \gamma_2) \cos \gamma_2 d\gamma_2 \right] d\gamma_1 \right)^2 = 0 \right. \quad (5)$$

where  $A_2 = A_{sp}$  and  $A_{20} = A_0$  for 2<sup>nd</sup> mode. The unknowns to be found from (3) are in bold font.

The equations (3) – (5) describing the single and bimodal excitations in the conservative and dissipative (not shown here) cases show that in both cases the problem is confined to finding the force and further extraction of the sample properties. Therefore, we might not expect new information from the bimodal excitation, and the contrast improvement can be due to the specifics of the 2<sup>nd</sup> mode, which is characterized by higher optical sensitivity than the 1<sup>st</sup> mode.

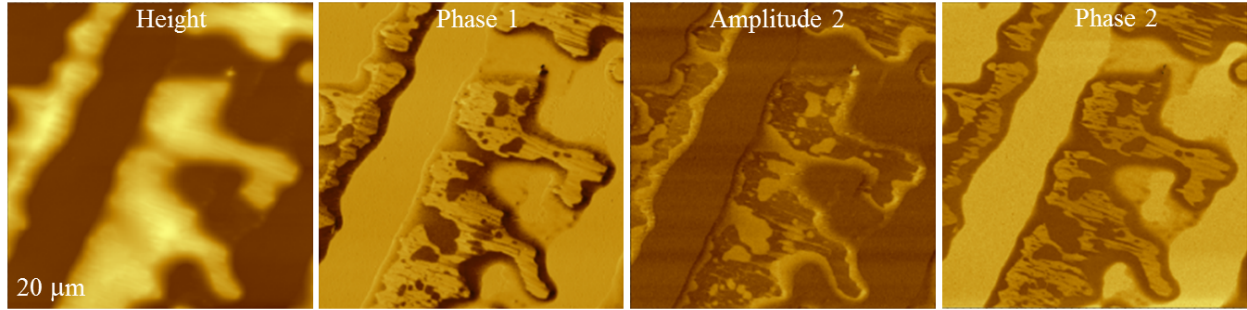


**Figure 6.** AFM images of PDES obtained in the bimodal excitation.

## CONCLUSIONS

Optimization of AFM measurements and data analysis gains substantial support from the theoretical consideration of tip-sample force interactions. We have illustrated this concept by several examples including high-resolution imaging, the comparison of resonant and non-resonant imaging modes, the problems of dissipative force interactions and bimodal excitation.

## REFERENCES

1. S. Belikov, and S. Magonov, *Amer. Control Confer.* 979 (2009).
2. S. Belikov, and S. Magonov, *Japan. Journ. Appl. Phys.* **45**, 2158 (2006).
3. S. Belikov, J. Alexander, S. Magonov, and I. Yermolenko, *Amer. Control Confer.* 3228(2012).
4. P. L. de Pablo, J. Colchero, J. Gomez-Herrero, and A. M. Baro, *Appl. Phys. Lett.* **73**, 3300 (1998).
5. S. Magonov, V. Elings, J. Cleveland, D. Denley, and M.-H. Whangbo, *Surface Science* **389**, 201 (1997).
6. R. Proksch, and D. Yablou, *App. Phys. Lett.* **100**, 073106 (2012).
7. C. Basire, and C. Fretigny, *C. R. Academie. Sci. Paris* **B325**, 211 (1997).
8. N. F. Martinez, S. Patil, J. R. Lozano, and R. Garcia, *Appl. Phys. Lett.* **89**, 153115 (2006).
9. S. Magonov, V. Elings, and V. Papkov, *Polymer* **38**, 297 (1997).